208

The Open Bioinformatics Journal

BENTHAM OPEN

CrossMark

RESEARCH ARTICLE

Electrocardiogram Fiducial Points Detection and Estimation Methodology for Automatic Diagnose

René Yáñez de la Rivera[1], Moisés Soto-Bajo[2,*] and Andrés Fraguela-Collar[1]

[1]*Facultad de Ciencias Físico-Matemáticas, Benemérita Universidad Autónoma de Puebla, Avenida San Claudio y 18 Sur, Colonia San Manuel, 72570 Puebla, México*

[2]*Cátedras CONACYT - Benemérita Universidad Autónoma de Puebla. Facultad de Ciencias Físico-Matemáticas, Benemérita Universidad Autónoma de Puebla, Avenida San Claudio y 18 Sur, Colonia San Manuel, 72570 Puebla, México*

Abstract:

Background:

The estimation of fiducial points is specially important in the analysis and automatic diagnose of Electrocardiographic (ECG) signals.

Objective:

A new algorithm which could be easily implemented is presented to accomplish this task.

Methods:

Its methodology is rather simple, and starts from some ideas available in the literature combined with new approachs provided by the authors. First, a *QRS* complex detection algorithm is presented based on the computation of energy maxima in ECG signals which allow the measurement of cardiac frequency (in beats per minute) and the estimation of R peaks temporal positions (in number of samples). From these ones, an estimation of fiducial points Q, S, J, P and T waves onset and offset points are worked out, supported in a simple modified slope method with constraints.

The location process of fiducial points is assisted with the help of the so called curvature filters, which allow to improve the accuracy in this task.

Results:

The procedure is simulated in Matlab and GNU Octave by using test signals from the MIT medical database, Cardiosim II equipment patterns and synthetic signals developed by the authors.

Conclusion:

One of the novelties of this work is the global strategy. Also, another significant innovation is the introduction of the curvature filters. We think this concept will prove to be a useful tool in signal processing, not only in ECG analysis.

Keywords: Automatic diagnose, Curvature filters, Electrocardiographic signal, Fiducial points, P wave, QRS complex, T wave, Signal processing.

* Address correspondence to the author at the Cátedras CONACYT - Benemérita Universidad Autónoma de Puebla. Facultad de Ciencias Físico-Matemáticas, Benemérita Universidad Autónoma de Puebla, Avenida San Claudio y 18 Sur, Colonia San Manuel, 72570 Puebla, México; E-mail: moises.soto@fcfm.buap.mx

1. INTRODUCTION

Electrocardiographic signals (ECG) are a main tool in Medicine, since ECG analysis is a routinary part of any complete medical evaluation. This is due to the fundamental role the heart plays in human health, and because ECG provides a noni nvasive and relatively easy way of knowing how the heart is working [1 - 8].

Furthermore, recently ECG and EEG (electroencephalographic) signals have proven to be an appropriate tool in fields as security, privacy, communication networks or psychology, in which biometric methods play a role [9 - 16].

In this context, the estimation of fiducial points of ECG signals is basic for feature extraction, and subsequently, to ECG interpretation. Thus, algorithms and techniques which could accomplish accurately this task are especially important in designing automatic analysis and diagnose tools.

A lot of such methodologies have been developed in the recent decades, which constitutes an active area of research, with multiple challenges still to overcome [1 - 4, 17 - 69]. The current work is a contribution to this goal.

Before to expose our method, let us describe the basic features of an ECG. In the Fig. (**1**) a typical cycle of an ECG with normal sinus rhythm is shown, with the P, Q, R, S and T waves. In this text, the starting and ending points of P and T waves are labeled P_i, P_f, T_i, and T_f, and its maximum/minimum as P_m and T_m, respectively. The starting point of the QRS complex is labeled Q_i, and the ending point J, as is known as the J point. Also, the maximum/minimum of the Q, R and S waves are labeled Q_m, R_m and S_m, respectively. Note that, because of its inherent complexity, there are no rigorous definitions of these concepts.
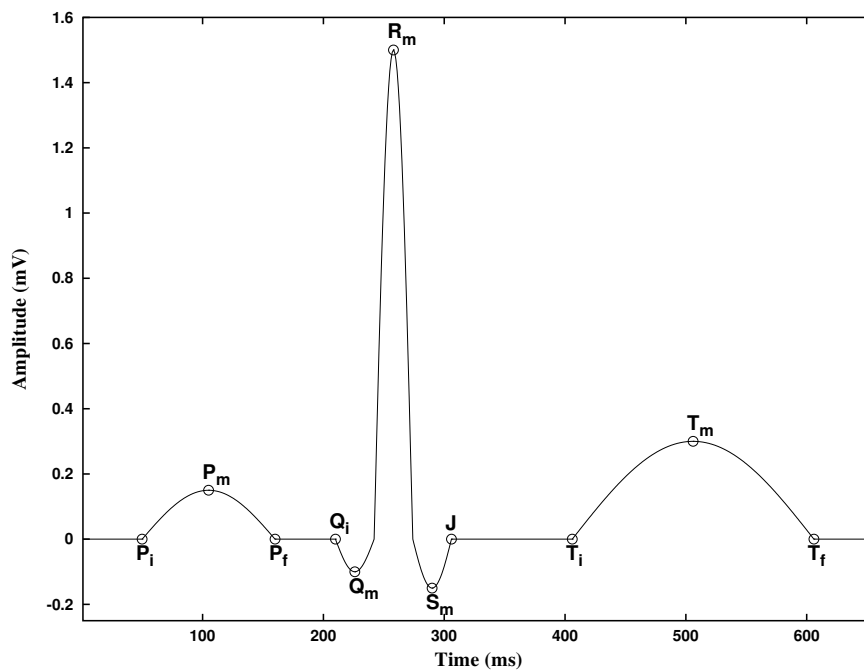

Fig. (1). Eschematic view of a cycle of an ECG with its fiducial points.

In addition, the piece of the signal between two consecutive R_m points is known as RR interval. Furthermore, the piece of the signal between P_i and the following Q_i point is known as PQ (or PR) interval, and the piece of the signal between Q_i and the following T_f point is known as QT interval. Analogously, the piece of the signal between the J point and the following T_i point is known as ST segment, and the piece of the signal between P_f and the following Q_i point is known as PQ segment [2].

The Table **1** shows the normal values of the main ECG features of a typical lead II in sinus rhythm at a heart rate of 60 *bpm* for a healthy male adult [2, 23, 70]. We will use these values for testing our methodology by simulating it in practical examples.

Table 1. Normal values and limits of the main ECG features.

Feature	Normal Value	Normal Limit
P width (P_f - P_i)	110ms	$\pm$20ms
PQ/PR interval (Q_i - P_i)	160ms	$\pm$40ms
QRS width (J - Q_i)	100ms	$\pm$20ms
QT interval (T_f - Q_i)	400ms	$\pm$40ms
ST segment (T_i - J)	150ms	-
T width (T_f - T_i)	150ms	-
P amplitude	0.15mV	$\pm$0.05mV
QRS height	1.50mV	$\pm$0.50mV
ST level	0.00mV	$\pm$0.10mV
T amplitude	0.30mV	$\pm$0.20mV

In the clinical evaluation of an ECG, physicians currently focus on the following main features [71, 72]:

1.1 Measurement of Cardiac Frequency: It consists on measuring the number of cycles or heartbeats per minute.

1.2 Heart Rate Analysis: The cardiac frequency should be almost constant in a sinus rhythm, when the sinoatrial node acts as the natural pacemaker. In the ECG, this is basically characterized by the fact that each *QRS* complex is preceded by a P wave.

1.3 Measurement of PR Interval: The PR interval measures the required time for the electrical impulse to traveling from the sinoatrial node to the ventricles. In a health individual, its length is between 120 ms and 200 ms. It is useful to evaluate the signal conduction in the atriums and it could help to identify atrial blocks.

1.4 Heart Vector Estimation: It is computed from I and III (or I and aVF) leads, and it gives information about blocks and hypertrophies.

1.5 Measurement of QT Interval: It gives information about depolarization and repolarization processes of ventricles, and it is related to some abnormalities known as QT syndrome.

1.6 Width of *QRS* Complex: It represents the time in which ventricles depolarizate, and it is estimated between 80 ms and 120 ms. It is useful to evaluate troubles in the conduction system, as blocks.

1.7 ST Segment: Its width is measured, as well as possible elevation or depression. It is related to ischemic processes, infarcts and other special diseases, as the Brugada syndrome.

8. Special Features of P, Q, R, S and T Waves: Some morphologies are connected to different pathologies.

Note that the diagnose of ECG signals is out of the scope of the current work, so the previous comments are merely orientative. Here we present a methodology for ECG analysis, focusing in the above 1, 2, 3, 5, 6 and 7 points.

2. MATERIALS AND METHODS

2.1. Curvature Filters

Before to proceed to explain the proposed method for ECG analysis, we introduce a new tool for signal analysis (to the best of our knowledge), which we call "curvature filters". We start by explaining the underlying idea.

The onset and offset of ECG waves are characterized by a noticeable change in the slope of the signal at these points. Usually R waves climb up or fall dramatically, what weakens the influence of noise and makes easier the work of locating them. However, in general these twists are not always easy to find, mainly because of the presence of noise. It is worth to note that noise makes an appropriate slope measurement greatly difficult.

The onset and offset of the P and T waves (here denoted P_i, P_f, T_i and T_f, respectively), as well as the onset of the Q wave (called Q_i) and the offset of the S wave, *i.e.*, the J point, sometimes are hard to be found. Frequently, the amplitude of the P wave (or even the T wave) is scarcely greater than the noise intensity. Often, this is also the case of Q and S waves, worsened by the fact of their much more short width. On the other hand, the T wave (and also the other waves) could be preceded or followed by ascending/descending periods of non vanishing slope, thus not completely isoelectric. These preceding periods are not quite different from the proper ascending/descending sides of the T wave. All these circumstances could collude in making these fiducial points almost indistinguishable from regular noise.

In order to be able to catch these twists, and taking into account the previously observed difficulty of measuring slopes under noise, we propose a technique to estimate "local curvature" of the signal.

In order to achieve this goal, we proceed as follows. We look for local information, but we have to average in order to avoid noise effects. On the other hand, the twists or slope changes we are looking for are linked in some sense to the second derivative, in "Calculus language". Thinking about Taylor approximations, this is nothing but approximate locally a function with second order polynomials. This way of thinking is merely motivational, since we are dealing with discrete signals. Nevertheless, we have found it useful in our simulations. Anyway, consequently, we have to discretize our approximations.

Fix a non negative integer $n \geq 3$, which will play the role of the window width. The set of integers will be denoted by $\mathbb{Z}$, and the set of real numbers will be denoted by $\mathbb{R}$. We consider the basic quadratic polynomial $p(x) = 3x^2$ on the interval $[-n, n]$ (the factor 3 is suitable for notation only), and we discretize it by averaging on uniform intervals of length two: For each integer k with $1 \leq k \leq n$ we compute:

$$\int_{-n+2(k-1)}^{-n+2k} p(x)\,dx = (2k-n)^3 - (2k-n-2)^3 = 6n^2 + 12n - 24nk + 24k^2 - 24k + 8. \tag{1}$$

Thus, we define

$$p_{n,k} = \frac{1}{4}\int_{-n+2(k-1)}^{-n+2k} p(x)\,dx = \frac{3}{2}n^2 + 3n - 6nk + 6k^2 - 6k + 2. \tag{2}$$

In order to make the curvature filter orthogonal to constant signals, we subtract the mean

$$\overline{p}_n = \frac{1}{n}\sum_{\nu=1}^{n} p_{n,\nu} = \frac{1}{4n}\int_{-n}^{n} p(x)\,dx = \frac{n^2}{2}. \tag{3}$$

Thus, we define for k with $1 \leq k \leq n$

$$f_{n,k} = p_{n,k} - \overline{p}_n = n^2 + 3n - 6nk + 6k^2 - 6k + 2. \tag{4}$$

We also set $\widetilde{f}_n = (\widetilde{f}_{n,1}, \ldots, f_{n,n}) \in \mathbb{R}^n$. Now we get $\sum_{\nu=1}^{n} f_{n,\nu} = 0$ from the above computations. One can also check that

$$f_{n,k} = 6\left(k - \frac{n+1}{2}\right)^2 - \frac{n^2-1}{2} \qquad (1 \leq k \leq n). \tag{5}$$

Note that $\widetilde{f}_{n,k}$ is integer for $k=1,\ldots,n$. For the sake of simplicity, the n-th curvature filter is defined by

$$f_n = (f_{n,1}, \ldots, f_{n,n}) = \lambda_n^{-1}\widetilde{f}_n \in \mathbb{R}^n, \tag{6}$$

where the positive integer factor λ^n is chosen such that the set of integers $\{f_{n,k}\}_{k=1}^{n}$ is mutually prime (the only positive integer that divides both of them is one). That reduces the size of the filter entries, and does not impact on their use, since any multiple of the curvature filter is equally useful as long as only one order n is used to measure local curvature.

It turns out that the sequence of scaling factors $\{\lambda_n\}_{n=3}^{\infty} \subset \mathbb{Z}$ is easily computed:

Proposition 2.1 The scaling factors in the definition of curvature filters (6) are given by

$$\lambda_{12m+p} = \begin{cases} 2 & \text{if } p = 0,3,9. \\ 4 & \text{if } p = 6. \\ 6 & \text{if } p = 1,4,5,7,8,11. \\ 12 & \text{if } p = 2,10. \end{cases} \tag{7}$$

for any m, $p \in \mathbb{Z}$ such that $0 \le p \le 12$ and $n = 12m + p \ge 3$.

We postpone its proof until Appendix A, in order to avoid a disruption in the explanation. Explicit expressions for the curvature filters can be found into this proof, and examples of the first curvature filters can be found listed in Table **2** at Appendix B.

Table 2. First curvature filters for 3 ≤ n ≤ 25.

n	3	4	5	6	7	8	9	10	11	12	13	14	15	16	17	18	19	20	21	22	23	24	25
$\|f_n\|^2$	6	4	14	84	84	168	2772	132	858	12012	2002	728	37128	5712	7752	23256	13566	17556	201894	7084	35420	394680	53820
1	1	1	2	5	5	7	28	6	15	55	22	13	91	35	40	68	51	57	190	35	77	253	92
2	-2	-1	-1	-1	0	1	7	2	6	25	11	7	52	21	25	44	34	39	133	25	56	187	69
3	1	-1	-2	-4	-3	-3	-8	-1	-1	1	2	2	19	9	12	23	19	23	82	16	37	127	48
4	-	1	-1	-4	-4	-5	-17	-3	-6	-5	-5	-2	-8	-1	1	5	6	9	37	8	20	73	29
5	-	-	2	-1	-3	-5	-20	-4	-9	-10	-10	-5	-29	-9	-8	10	-5	-3	-2	1	5	25	12
6	-	-	-	5	0	-3	-17	-4	-10	-35	-13	-7	-44	-15	-15	-22	-14	-13	-35	-5	-8	-17	-3
7	-	-	-	-	5	1	-8	-3	-9	-35	-14	-8	-53	-19	-20	-31	-21	-21	-62	-10	-19	-53	-16
8	-	-	-	-	-	7	7	-1	-6	-29	-13	-8	-56	-21	-23	-37	-26	-27	-83	-14	-28	-83	-27
9	-	-	-	-	-	-	28	2	-1	-17	-10	-7	-53	-21	-24	-40	-29	-31	-98	-17	-35	-107	-36
10	-	-	-	-	-	-	-	6	6	1	-5	-5	-44	-19	-23	-40	-30	-33	-107	-19	-40	-125	-43
11	-	-	-	-	-	-	-	-	15	25	2	-2	-29	-15	-20	-37	-29	-33	-110	-20	-43	-137	-48
12	-	-	-	-	-	-	-	-	-	55	11	2	-8	-9	-15	-31	-26	-31	-107	-20	-44	-143	-51
13	-	-	-	-	-	-	-	-	-	-	22	7	19	-1	-8	-22	-21	-27	-98	-19	-43	-143	-52
14	-	-	-	-	-	-	-	-	-	-	-	13	52	9	1	-10	-14	-21	-83	-17	-40	-137	-51
15	-	-	-	-	-	-	-	-	-	-	-	-	91	21	12	5	-5	-13	-62	-14	-35	-125	-48
16	-	-	-	-	-	-	-	-	-	-	-	-	-	35	25	23	6	-3	-35	-10	-28	-107	-43
17	-	-	-	-	-	-	-	-	-	-	-	-	-	-	40	44	19	9	-2	-5	-19	-83	-36
18	-	-	-	-	-	-	-	-	-	-	-	-	-	-	-	68	34	23	37	1	-8	-53	-27
19	-	-	-	-	-	-	-	-	-	-	-	-	-	-	-	-	51	39	82	8	5	-17	-16
20	-	-	-	-	-	-	-	-	-	-	-	-	-	-	-	-	-	57	133	16	20	25	-3
21	-	-	-	-	-	-	-	-	-	-	-	-	-	-	-	-	-	-	190	25	37	73	12
22	-	-	-	-	-	-	-	-	-	-	-	-	-	-	-	-	-	-	-	35	56	127	29
23	-	-	-	-	-	-	-	-	-	-	-	-	-	-	-	-	-	-	-	-	77	187	48
24	-	-	-	-	-	-	-	-	-	-	-	-	-	-	-	-	-	-	-	-	-	253	69
25	-	-	-	-	-	-	-	-	-	-	-	-	-	-	-	-	-	-	-	-	-	-	92

Each column lists the order *n*, the size $\|f_n\|^2$, and the filter entries $f_{n,k}$ (for $k = 1,...,n$).

In virtue of identity (5) the filter entries are symmetric with respect to $(n+1)/2$. Consequently, the curvature filter is also orthogonal to linear signals. It is worth to note that symmetry implies that only the half of filter entries $f_{n,k}$ need to be computed.

Given a signal $s = \{s_v\}_{v \in \mathbb{Z}} \subset \mathbb{R}$, for any $k \in \mathbb{Z}$ its *k*-th curvature coefficient of order n is

$$c_{n,k}(s) = \sum_{v=-(n-1)/2}^{(n-1)/2} s_{k+v} f_{n,(n+1)/2+v} \tag{8}$$

if *n* is odd, and

$$c_{n,k}(s) = \sum_{v=-n/2+1}^{n/2} s_{k+v} f_{n,n/2+v} \tag{9}$$

if *n* is even.

Because of the above computations, the curvature filter f_n is orthogonal to affine signals: for any $\lambda, \mu \in \mathbb{R}$ we have

$$\sum_{v=1}^{n} (\lambda\, v + \mu)\, f_{n,v} = 0. \tag{10}$$

That means that the curvature coefficients are insensitive to the signal level and slope. This property is important, since we want the curvature filters for measuring only slope changes, not the slope or the proper signal itself.

If one wants to use only curvature coefficients of the same order, these definitions with integer $f_{n,k}$ are enough. However, if one wants to compare curvature features corresponding to different orders n, an appropriate normalization is convenient.

We define the normalized curvature filter $F_n = (F_{n,1}, \ldots, F_{n,n}) \in \mathbb{R}^n$ by

$$F_n = \frac{1}{\|f_n\|}\, f_n = \frac{1}{\left(\sum_{v=1}^{n} |f_{n,v}|^2\right)^{1/2}}\, f_n. \tag{11}$$

Given a signal $s = \{s_v\}_{v \in \mathbb{Z}} \subset \mathbb{R}$, for any $k \in \mathbb{Z}$ its k-th normalized curvature coefficient of order n is

$$C_{n,k}(s) = \frac{c_{n,k}(s)}{\|f_n\|}. \tag{12}$$

Explicit expressions can be also easily found for the normalized curvature filters:

Theorem 2.2 For any $n \geq 3$ the normalized curvature filter entries are given (for $1 \leq k \leq n$) by

$$F_{n,k} = \frac{\sqrt{5}\,(n^2 + 3n - 6nk + 6k^2 - 6k + 2)}{(n^5 - 5n^3 + 4n)^{1/2}} = \frac{\sqrt{5}\left[6\left(k - \frac{n+1}{2}\right)^2 - \frac{n^2-1}{2}\right]}{[(n-2)(n-1)n(n+1)(n+2)]^{1/2}}. \tag{13}$$

These formulae come from (4), (5), and the following result.

Proposition 2.3 For any integer $n \geq 3$ one has

$$\|\widetilde{f}_n\|^2 = \sum_{v=1}^{n} |\widetilde{f}_{n,v}|^2 = \frac{n^5 - 5n^3 + 4n}{5} = \frac{(n-2)(n-1)n(n+1)(n+2)}{5}. \tag{14}$$

We postpone its proof until Appendix A, in order to avoid a disruption in the explanation.

2.1.1.. Choice of curvature filter orders

In order to obtain an accurate result in using curvature filters for wave onset and offset estimation, an appropriate order n must be chosen on each case. In this section we argue about how to choose this optimal order. In order to do that, we test the curvature filters on a test example designed for offset estimation. The picture for onsets is completely similar because of symmetry.

We fix a time wave length w_t, in milliseconds, and a corresponding wave length w_s, in number of samples. The estimated sampling frequency is then obtained by the formula $F_s \sim 1000 w_s/w_t$, in Hertzs, where this quantity is rounded to the closest integer. The base signal is composed by a semi ellipse of length w_s samples and height h (in millivolts), followed by w_s zeroes. Consequently, the signal length is $2w_s$. The base signal is perturbed with random noise of a given intensity h_n (in millivolts), giving a set of N_t perturbed signals of length $2w_s$.

In the next test example we use the following values: w_t=110 *ms*, h=0.15 *mV*, h_n=0.01 *mV*, and N_t=100 signals (according to the *P* wave in the Table **1**). The wave lengths used to test the curvature filters in this example go from w_s=3 samples up to w_s=100 samples, by increments of 1 sample.

Next, for each noisy signal s_j (with j=1,...,N_t), and for each order n (with n=3,...,$2w_s$-1), we compute the corresponding normalized curvature coefficients. Note that we do that only for sample points such that the window is completely included into the signal range, as we are dealing with a finite signal; that depends on the order n of the

curvature filter used. Then, we estimate the offset by selecting the greatest normalized curvature coefficient; thus, its offset is defined as the corresponding sample point $k=o_{j,n}$ with greatest normalized curvature coefficient. Note that, as we are looking for offsets for upward waves, we might select points with maximum convexity; *i.e.*, greatest positive curvature.

In Figs. (**2** and **3**) we show the resulting estimated offsets $o_{j,n}$ for $j=1,...,N_t$, and $n=3,...,2w_s-1$, for the wave lengths $w_s=15$ samples (corresponding to $F_s=136$ Hz) and $w_s=55$ samples (corresponding to $F_s=500$ Hz). We consider as a reference correct offset the sample point $k=w_s$.
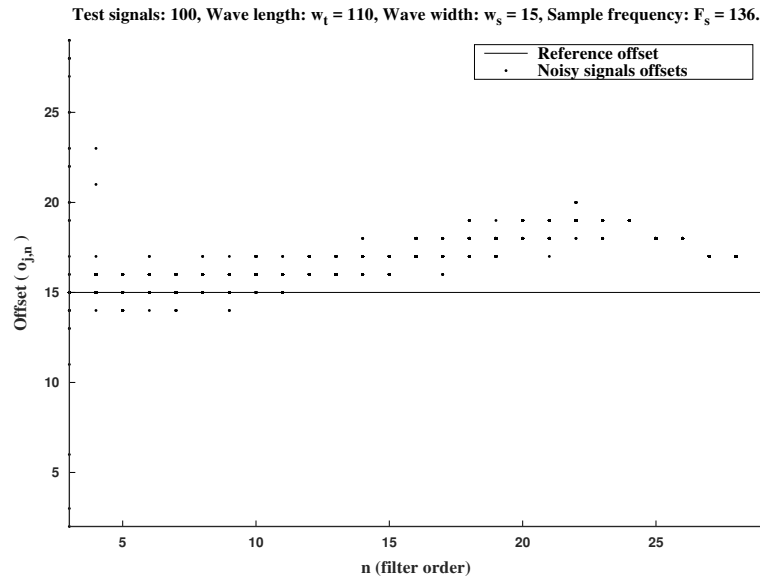
Fig. (2). Obtained offsets in the curvature filters order test for $w_s = 15$.
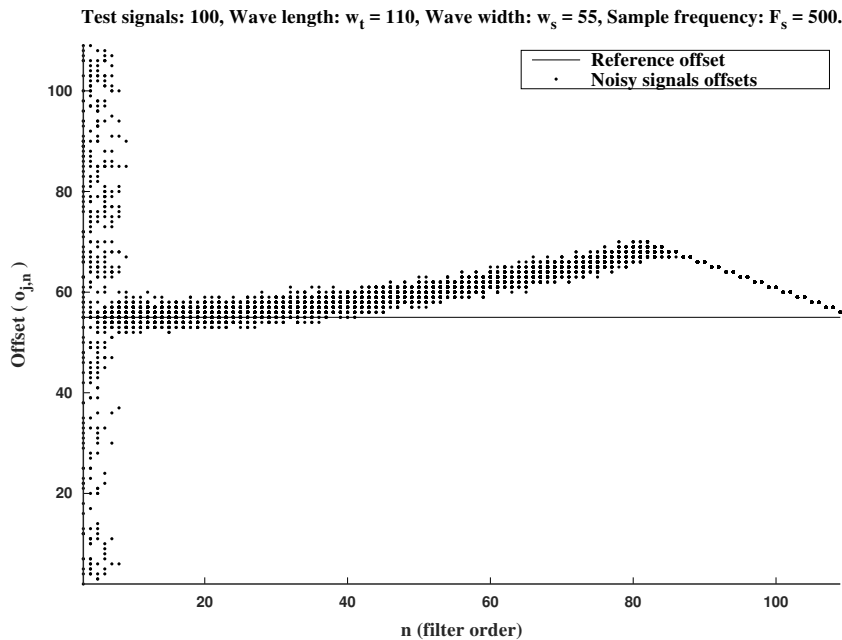
Fig. (3). Obtained offsets in the curvature filters order test for $w_s = 55$.

In view of Figs. (**2** and **3**) and the rest of simulations, several comments arise about the curvature filters performance:

• If the curvature filter order is too small, then the noise has a profound effect in the curvature coefficients. That

is, low order curvature filters do not distinguish between signal twists and noise.

- From certain large enough order, curvature filters are very proficient on the task of detecting the offset.
- The accuracy of the measurement slightly deteriorates as the order increases. On average, a trend to shift outwards the wave is detected.
- The latter convergence for very high orders is spurious since is due to the finite character of the signal.

These remarks suggest that curvature filters could be an useful tool on detecting fiducial points in ECG signals, provided that a suitable order is chosen for the specific task. We think this is valid also for features extraction in signal processing, in general.

In order to measure quantitatively the curvature filters performance in the test example, we define the error as $\varepsilon_{j,n} = |o_{j,n} - w_s|$ (w_s being fixed), for any $j=1,...,N_t$, and n=3,...,2w_s-1. Thus, for each order n we compute the mean error

$$\varepsilon_n = mean((\varepsilon_{j,n})_{j=1,...,N_t}) = \frac{1}{N_t} \sum_{j=1}^{N_t} \varepsilon_{j,n} \,. \tag{15}$$

Then, the mean optimal order is defined as the (smallest) order $n=n_m$ for which ε_n is minimum ($\varepsilon_{n_m} \leq \varepsilon_n$ for all $n = 3, \ldots, w_s$).   In other words, the mean optimal order is the window size for which the greatest-curvature-coefficient method (*i.e.*, the previous one) for detecting the offset is more accurate, on average. Note we avoid too large orders in this criteria.

Another important features which are also highly desirable, apart from accuracy, are fiability and robustness under noise presence. In order to take into account these aspects, we also analyse the measurements error dispersion provided by the greatest-curvature-coefficient method. Hence, we consider the error standard deviation

$$\sigma_n = std((\varepsilon_{j,n})_{j=1,...,N_t}) = \sqrt{\frac{1}{N_t} \sum_{j=1}^{N_t} (\varepsilon_{j,n} - \varepsilon_n)^2} \,. \tag{16}$$

In Figs. (**4** and **5**) we see that the magnitude of the errors dramatically falls off after the initial noise-sensitive period, as expected from the above remarks based on Figs. (**2** and **3**) Coherently, the mean error ε_n and the error standard deviation σ_n also have the same behavior. We define the standard deviation optimal order as the first order $n=n_{std}$ such that $\sigma_n \leq \sigma_{n+1}$ and σ_n is lower than a reference value empirically set to 2. That is, we look for a small enough local minimum of the standard deviation.
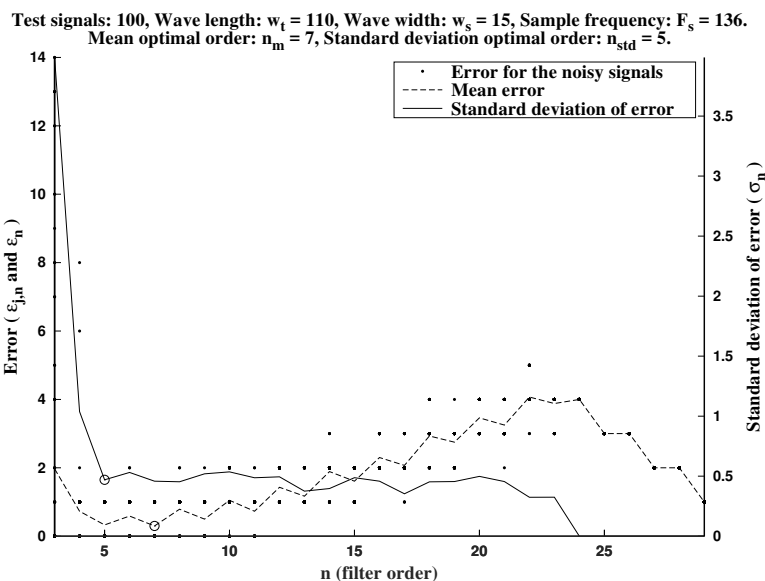

Fig. (4). Obtained errors, mean error and error standard deviation in the curvature filters order test for $w_s = 15$.

Test signals: 100, Wave length: w$_t$ = 110, Wave width: w$_s$ = 55, Sample frequency: F$_s$ = 500.
Mean optimal order: n$_m$ = 15, Standard deviation optimal order: n$_{std}$ = 11.
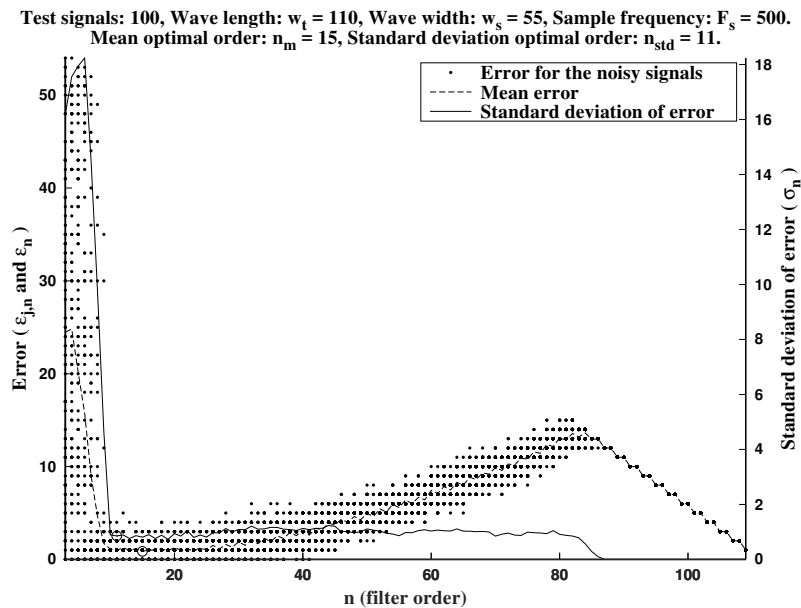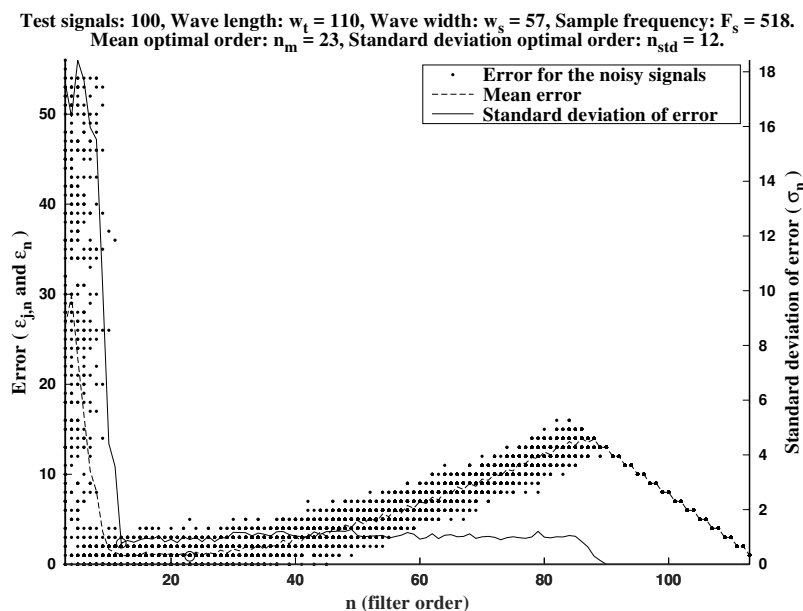

Fig. (5). Obtained errors, mean error and error standard deviation in the curvature filters order test for w_s = 55.

As it has been remarked before, immediately after the initial noise-sensitive period the greatest-curvature-coefficient method performs very well, providing a quite low mean error almost stagnant in a long period on n. The same could be said for the standard deviation of the error.

As it is illustrated in Fig. (**6**), it often occurs that the mean optimal order unnecessarily increases to larger values. Due to computational reasons, it is preferable to use low order filters as long as possible. Another factor to bear in mind is that, generally, waves do not occur isolated in an ECG, but surrounded by other ones. Hence, too high orders are undesirable since the presence of neighboring waves could cause interference.

Test signals: 100, Wave length: w$_t$ = 110, Wave width: w$_s$ = 57, Sample frequency: F$_s$ = 518.
Mean optimal order: n$_m$ = 23, Standard deviation optimal order: n$_{std}$ = 12.

Fig. (6). Obtained errors, mean error and error standard deviation in the curvature filters order test for w_s = 57.

In order to avoid that, we recommend as a preferential choice the standard deviation optimal order n_{std} to be used in the greatest-curvature-coefficient method.

In Fig. (**7**) we can see the optimal orders (mean optimal order n_m and standard deviation optimal order n_{std}) for w_s in the proposed range (that is, wave lengths from w_s=3 samples up to w_s=100 samples, by increments of 1 sample).
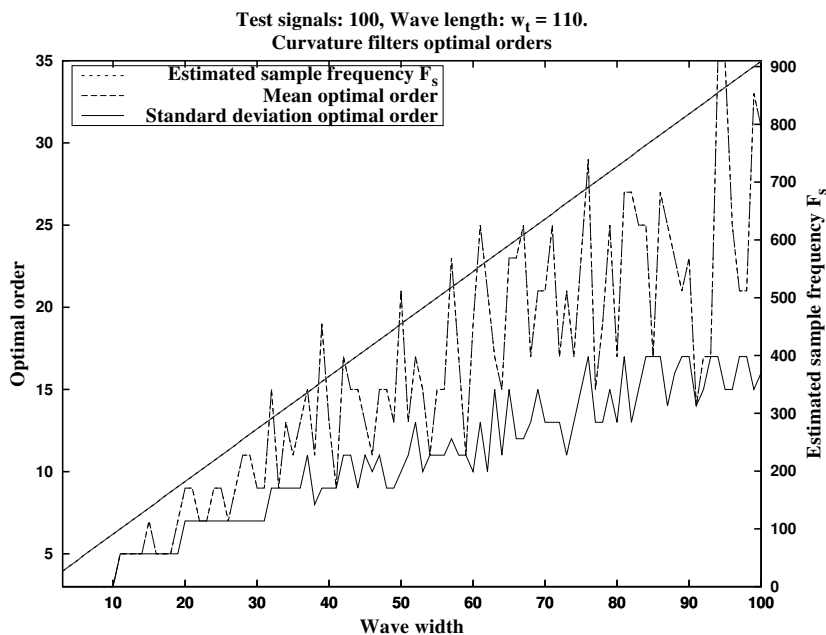
Fig. (7). Optimal (mean and standard deviation) orders obtained in the curvature filters order test.

In summary, in view of Fig. (**8**), we recommend to use a curvature filter order between the 15% and the 30% of the wave width w_s. These values should be increased for very low sampling frequencies, as the resulting from Holter monitors. This quantity could be estimated a priori from the estimated wave length w_t (in milliseconds, which could be taken from references as in Table **1**), and the signal sampling frequency F_s (in Hertz), which is assumed to be known, by the formula.

$$w_s \sim \frac{w_t \, F_s}{1000}.$$

$$(17)$$
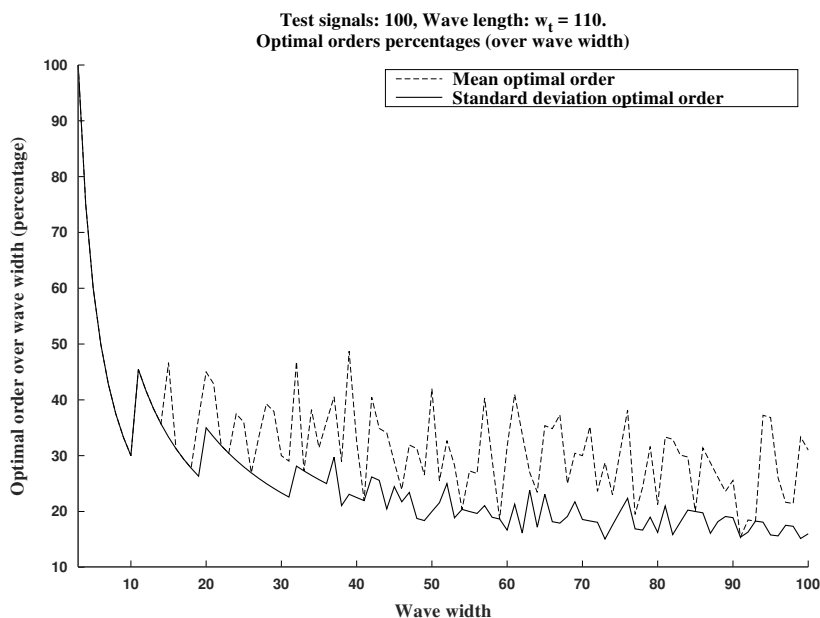
Fig. (8). Quotients of optimal (mean and standard deviation) orders obtained in the curvature filters order test with respect to w_s (in percentages).

2.2. Description of Methodology

In this section we will describe our proposal of methodology for the analysis and features extraction of ECG signals.

Suppose we have a non trivial ECG signal, denoted $ecg0$, of length L. That is, $0 \neq ecg0 = (ecg_{0,1}, \ldots, ecg_{0,L}) \in \mathbb{R}^L$ is a vector of L real components. We will denote by F_s the sample rate (sampling frequency) with which the ECG signal was taken, measured in Hertzs (Hz).

2.2.1. Preprocessing

Generally, the ECG signal is assumed to be contaminated with several noise sources. This noise could be reduced by using some filters which cut off different frequencies, but definitely cannot be completely avoided. Anyway, for this reason and previous to the feature extraction process, a preprocessing is necessary to be applied to the signal. Consequently, the original signal suffers changes which add some uncertainty to the final results. This phenomena is specially remarkable in the case of P and T waves onset and offset location. That is why we speak about feature ``estimation'', and not about ``measurement''.

First of all, the amplitude of the original signal is normalized to 1:

$$ecg1 = \frac{1}{\max_{1 \leq k \leq L} |ecg_{0,k}|} \, ecg0. \tag{18}$$

The resulting signal $ecg1 = (ecg_{1,1}, \ldots, ecg_{1,L}) \in \mathbb{R}^L$ has amplitude 1. Next, the direct level is supressed, obtaining a signal $ecg2 = (ecg_{2,1}, \ldots, ecg_{2,L}) \in \mathbb{R}$ given by

$$ecg2 = ecg1 - mean(ecg1) = ecg1 - \frac{1}{L} \sum_{k=1}^{L} ecg_{1,k}. \tag{19}$$

Obviously, one has mean($ecg2$)=0.

After that, a high pass filter of type Butterworth of order 2 is applied to filter $ecg2$, with a cut frequency of 0.5 Hz, to obtain a preprocessed signal $ecg3 = (ecg_{3,1}, \ldots, ecg_{3,L}) \in \mathbb{R}^L$. This step is always present in ECG professional applications, in order to remove very low frequencies.

When applying this preprocessing to signals from the MIT database ([73]), which proceed from Holters, this last step is very important and helps to improve the accuracy in subsequent estimations. On the other hand, when dealing with signals from pattern generating devices, it is usually required an additional filtering of smoothing or averaging type. In general, the required preprocessing highly depends on the measurement system features used to generate the ECG signal, and could include the use of other filters, as interference supressing filters out of 60 Hz. For the signals we have used in this work, this is not the case.

2.2.2. R_m Peaks Location and Heart Rate Analysis

QRS complex detection is considered a fundamental step in the analysis of ECG signals, because of measurement and characterization of different associated parameters rely on the accuracy with which it is performed (see [19], [2]). On the one hand, from the QRS complex cardiac frequency can be obtained, and subsequently heart rate is also obtained. On the other hand, R_m peaks almost delimitate each heart beat (more clearly than other waves) in such a way that estimation of the other fiducial points is more easily carried out from them.

In the recent decades many QRS complex detection methods have been reported in the literature (see [17], [18], [19], [1], [2], [24], [4], and references therein), including derivatives approximation, digital filters, wavelets, adaptative filters, neural networks, hidden Markov models or mathematical morphology, among other techniques.

In this work, we make use of the techniques developed in the literature [24]. Concretely, we select the preprocessed signal energy maximum, choosing a threshold which is empirically set. An appropriate choice of these maximum allows to obtain the heart rate (in beats per minute). Moreover, we describe two different methods to locate the R_m peaks in the original signal (in number of samples): one can simply extract the maximum peaks, or one can perform a crossed correlation between the filtered signal and the original signal (normalized and prefiltered).

We start with the preprocessed signal ecg3. Previous to energy processes, we filter it by using a band pass filter, in the band 10-25 Hz or 15-20 Hz, obtaining a filtered signal $ecg4 = (ecg_{4,1}, \ldots, ecg_{4,L}) \in \mathbb{R}^L$. This step is mandatory

in order to remove artifacts, interferences, and the influence of *P* and *T* waves. Note that in this moment we are only interested in detecting R_m peaks (Fig. **9**).
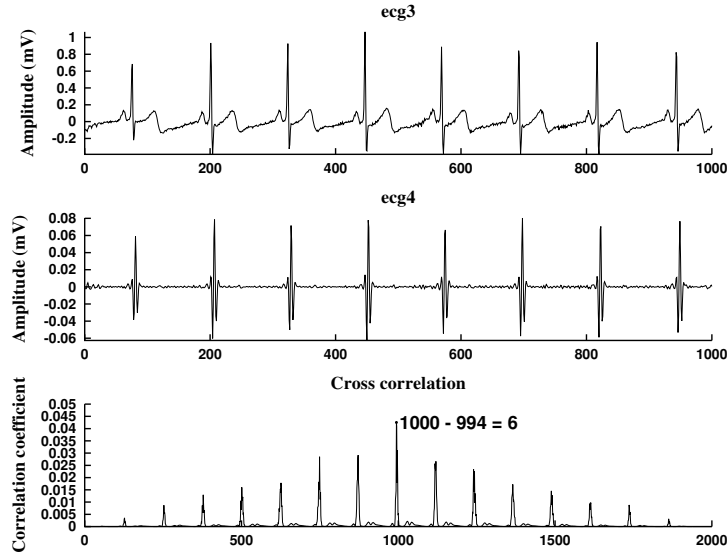

Fig. (9). Example of R_m peaks location by using the correlation technique.

Next, we consider the energy signal E_4 given by $E_4 = (|ecg_{4,1}|^2, \ldots, |ecg_{4,L}|^2) \in \mathbb{R}^L$. The energy threshold E_{th} is empirically set to the value

$$E_{th} = 2\,mean(E_4) = \frac{2}{L} \sum_{k=1}^{L} |ecg_{4,k}|^2 . \tag{20}$$

Then, the energy maximum are extracted with the constraint $E_4 > E_{th}$. In the MATLAB code, the energy peak extraction is performed by using the implemented built-in function *findpeaks* ([74]). The resulting energy peaks have to be sifted out, since they usually appear pairs of ``peaks" which are unnaturally quite close (presumably corresponding to the same R wave, due to the noise and filtering processes). These related peaks have to be removed, since they produce non physiological values for the cardiac frequency.

Each energy peak corresponds to an R_m peak, but the last ones need to be located, since the band pass filtering provokes a constant gap between the two signals, which shifts the peaks in time.

What we do is to compute the cross-correlation and finding the correlation coefficient between the energy E_4 of the

filtered signal and the energy E_3 (given by $E_3 = (|ecg_{3,1}|^2, \ldots, |ecg_{3,L}|^2) \in \mathbb{R}^L)$ of the original preprocessed signal. Then, the shift is the difference between the signal length L and the lag corresponding to the correlation coefficient K_{cr}, the maximum of the cross correlation. In that way, we are able to locate the R_m peaks in the original preprocessed signal *ecg*3. In the code, the cross-correlation analysis is performed by using the MATLAB built-in function *xcorr* ([74]).

Once the R_m peaks of ecg3 are located, the *RR* intervals are known. The widths of *RR* intervals, or distance between consecutive R_m peaks, allow to compute the approximated cardiac frequency: if L_{RR} is the width of a given *RR* interval (in number of samples), and *HR* is the heart rate (measured in beats per minute *bpm*), then

$$HR = \frac{60\,F_s}{L_{RR}} . \tag{21}$$

2.2.3. QRS Complex Location

In order to describe the *QRS* complex, we have to locate the Q_i, Q_m, S_m and *J* points of each cycle. Here, for exposition purposes, we consider the R_m point as the maximum of the *R* wave, and the Q_m and S_m points are understood as the minimum of the *Q* and *S* waves, respectively. In addition, Q_i is the starting point of the *Q* wave and the end of the

exposition purposes, we consider the R_m point as the maximum of the R wave, and the Q_m and S_m points are understood as the minimum of the Q and S waves, respectively. In addition, Q_i is the starting point of the Q wave and the end of the PQ segment, and J is the ending point of the S wave and the start of the ST segment.

For this task, we proceed by using a modified slope analysis method with restrictions, starting from a peak. This algorithm is inspired by Chapter 9 of [2]. The basic idea is to descend/ascend from a maximum/minimum, respectively, until a change in the sign of the slope is found. On a given sample point k (with $1 \leq k < L$), the slope of the signal *ecg3* is defined by

$$s_k = ecg_{3,k+1} - ecg_{3,k}.$$

(22)

This method is justified because of in the pronounced ascents and falls of the signal, the influence of the noise is quite lower than in the isolectric segments.

In this analysis we remove the first and final cycles, since they could be incomplete or distorted because of the original signal capture process. Then, consider the original preprocessed signal *ecg3*, and fix some R_m peak (not the first, not the last one).

On the one hand, we move backward from the R_m peak until we find the first local minimum; that is, until we find a point k whose left neighbor has nonpositive slope $s_{k-1} \leq 0$. This point is defined as the Q_m point of this cycle. From this point, we continue backward looking for the first local maximum; that is, a point k such that its left neighbor has nonnegative slope This point is defined as the $s_{k-1} \geq 0$. This point is defined as the Q_i point of this cycle.

On the other hand, we proceed analogously to the right. From the R_m peak, we move forward until we find the first local minimum; that is, until we find a point k with nonnegative slope $s_k \geq 0$. This point is defined as the s_m point of this cycle. From this point, we continue forward looking for the first local maximum; that is, a point k with nonpositive slope $s_k \leq 0$. This point is defined as the J point of this cycle.

In practice, this method needs to be complemented with different criteria about how far the search should go, related to the estimated length of the Q and S waves. This is because of, depending on the presence or absence of Q and S waves in the ECG signal, the pure slope analysis algorithm could produce fiducial points far away from the R_m peak, which would be unnatural. On the other hand, the greatest/smallest-curvature-coefficient method could assist the slope analysis method, as in the following subsection is illustrated, specially in the case of the Q_i and J points. However, the short width of these waves forces to use a quite small order, which could be imprecise, specially for signals with very low sampling frequency.

2.2.4. Estimation of Remaining Fiducial Points

At this point, what remains is to estimate the fiducial points in P and T waves. We proceed by using a modified slope analysis method [2], as before, combined with the use of curvature filters.

First of all, we find the P_m and T_m peaks. Without loss of generality, we assume we deal with upward P and T waves. The case of downward waves is completely analogous, and an algorithm to distinguish between upward and downward cases is easy to implement by computing maximum and minimum and comparing them (Q_i and J points could be taken as isoelectric reference level for the comparison, respectively).

Hence, from the R_m peak, we look for a global maximum in a preestablished backward/forward range of samples of the signal, respectively. This range could be estimated from the reference values for the PQ and QT intervals (Table **1**), the sampling frequency and the previously estimated fiducial points. Thus, the left maximum corresponds to P_m, and the right one corresponds to T_m.

From each one of these points, we descend in order to find the corresponding onset and offset points. The idea is to scan the surrounding signal looking for suitable candidates by using the slope analysis algorithm, and then selecting the best choice with the aid of the curvature filters. The process is as follows.

We start from the P_m point (the process for the T wave is completely analogous). On the one hand, we move backward inside a preestablished range looking for local minimum: Points k whose left neighbors have nonpositive slope $s_{k-1} \leq 0$. At each step, we store them as candidates. When the Range is exhausted, we select the winner by the greatest-curvature-coefficient method: We compute the curvature coefficients of the candidates, and the sample with

greatest one among them is designated as the P_i point of the cycle. On the other hand, from the P_m peak we move forward inside a preestablished range (never farther than the corresponding Q_i point) looking for local minimum: points k with nonnegative slope $s_k \geq 0$. They are the candidates, and the P_f is selected among them by the greatest-curvature-coefficient method.

Note that a stopping criteria is necessary in this algorithm. As before, the ranges could be estimated from the reference values for the *PQ* and *QT* intervals (Table **1**), the sampling frequency and the previously estimated fiducial points. Also, it could happen that candidates which are quite close to the P_m/T_m peaks, respectively, might have to be removed, as at the top of the *P* and *T* waves they could exist points with high curvature coefficients, specially in cases of nonstandard morphologies. Consequently, a starting criteria could be also necessary. On the other hand, suitable curvature filters orders for the *P* and *T* waves need to be chosen for a well performance of the algorithm (subsection 2.1.1.).

3. RESULTS

Next we show some examples of application of this methodology. For *QRS* complex detection, the modified slope analysis method was used, aided by range criteria based on estimated wave widths. For *P* and *T* waves estimation, a combined slope analysis and curvature filters method was used, aided with an starting/stopping criteria based on estimated wave widths (Table **1**). In the simulations presented here, the used curvature filters orders were *n*=3 for the *QRS* complex, and *n*=5 for the *P* and *T* waves, in the case of F_s=128 Hz, and n=9,11,13 for the *QRS* complex, *P* and *T* waves, respectively, in the case of F_s=500 *Hz* (Fig. **7**). Odd orders are prefered because of they center the fiducial point in a better way.

The first ECG signal is cs403, generated by a Cardiosim II device [75] by using the pattern 03, a reference pattern of a normal ECG. The second one is a synthetic ECG signal made by the authors, simulating also a normal sinus rhythm but without noise. Both have a heart rate of HR=60 bpm and a sampling frequency of F_s=500 *Hz* (Fig. **10**).
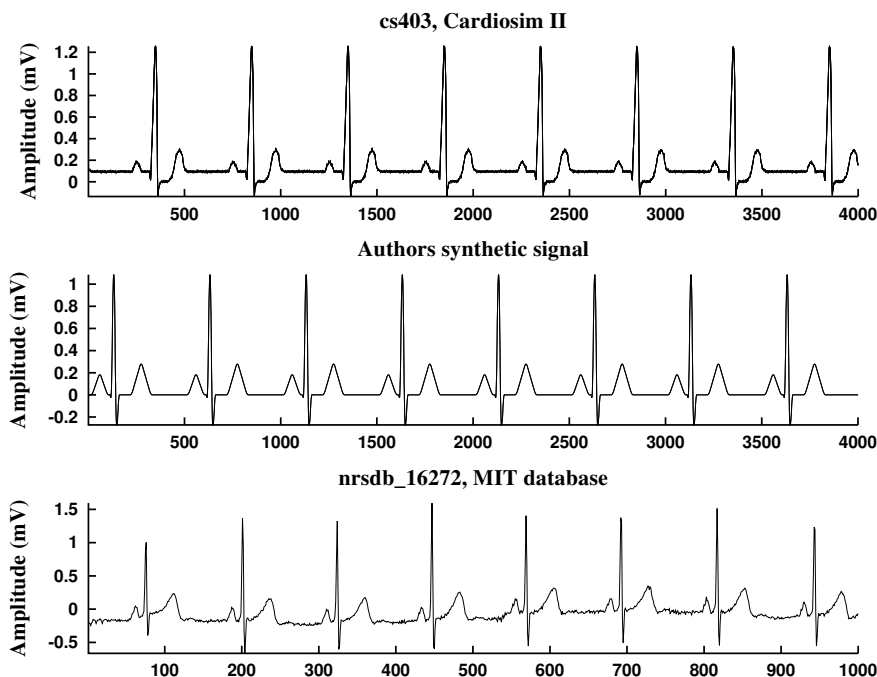
Fig. (10). Testing ECG signals.

As can be observed in Fig. (**11**), the signal slope, defined by (22), gives information about the increase of the ECG signal. However, in Figs. (**12**) it is clear that noise deeply affects to the signal slope. In that context, curvature filters help to avoid noise in order to find the fiducial points, since they regularize the signal. This effect is due to the fact that the curvature coefficients are weighted averages of the signal.
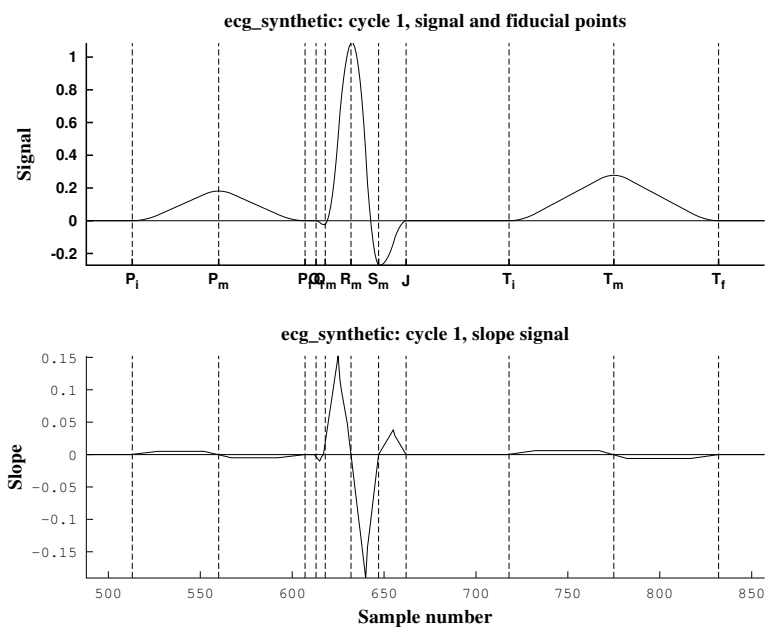
Fig. (11). Cycle of the synthetic signal, with estimated fiducial points.
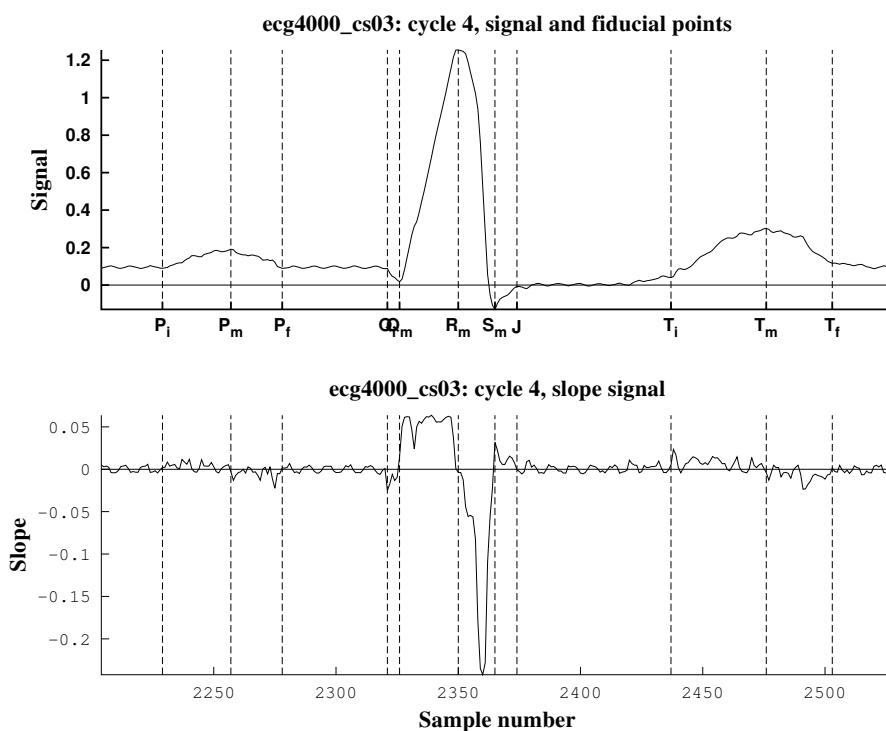

Fig. (12). Cycle of cs403 signal, with estimated fiducial points.

The third example is a piece of 8 cycles of nrsdb_16272, a real ECG signal from the normal sinus rhythm data base from the PhysioBank (MIT database [73]), reported with sampling frequency F_s=128 *Hz* and nominal *HR*=60 *bpm*. In Fig. (**13**) a cycle of this signal is shown, with estimated fiducial points.
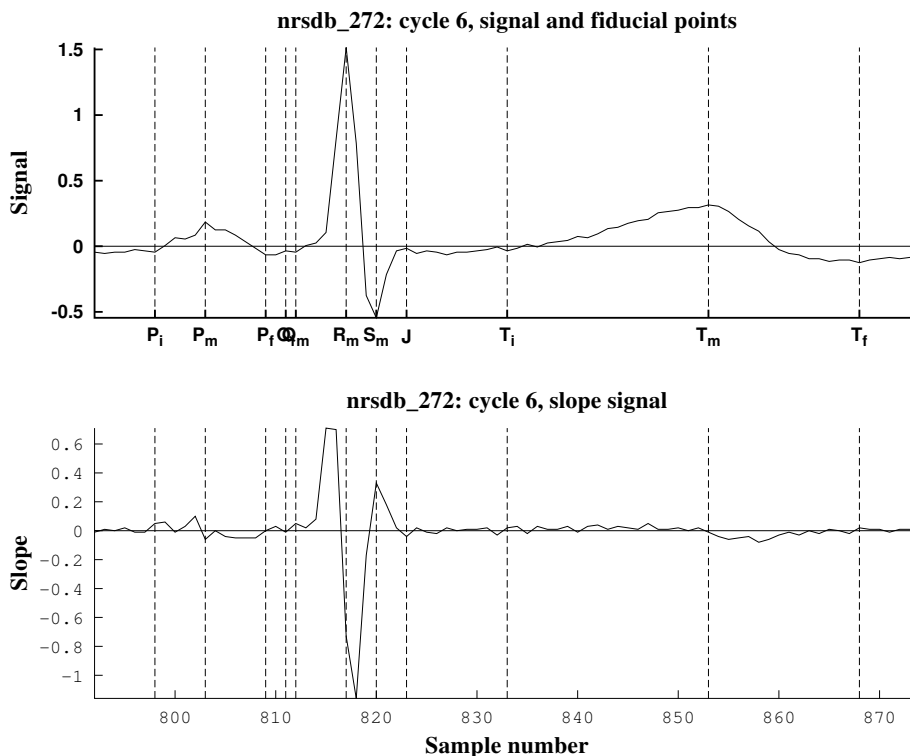
Fig. (13). Cycle of nrsdb 16272 signal, with estimated fiducial points.

All measurements have been taken with a level of noise, measured in the isoelectric segment which follows the *P* waveform, between P_f and Q_i, lower than $1.33 \times 10^{-4} mV^2/\Omega$ (a power of around 100 *pW*). This is equivalent to a signal contaminated with a maximum random noise of 0.01 *mV* in amplitude before the operation of prefiltering. That justifies the choice h_n at subsection 2.1.1.

From the standpoint of signal to noise ratio *S/N*, a good performance criterion is obtained with $S/N \geq 20 dB$, figure of merit kept also in the measurements above [23, 76, 77]. In all cases the power was estimated through the *var* function of Matlab which gives the signal variance [74].

4. DISCUSSION

Here we have presented a methodology for estimating the fiducial points of an ECG signal. Other features or measurements of interest, as widths of intervals and segments, wave heights, cardiac frequency, heart rate analysis can be computed from the located fiducial points.

One of the novelties of this work is the global strategy: first we localize the *R*, *P* and *T* waves peaks, and then we move backward/forward to the onset/offset, respectively. In this way, we are able to reduce the impact the noise has in the location process.

Also, another significant innovation is the introduction of the curvature filters. We think this concept will prove to be an useful tool in signal processing, not only in ECG analysis.

Moreover, it is worth to note that the combination of the greatest/smallest-curvature-coefficient method and the slope analysis method is significantly more effective than each of them separately: The first one adds accuracy and robustness to the second one, and the last one adds efficiency to the first one, as it reduces much more the number of curvature coefficients to be computed. Note that the signal slope is computationally cheaper than curvature coefficients.

It is worth to note that our method is specially designed to be applied to ECG signals corresponding to a normal sinus rhythm. However, we expect that the philosophy under the method, and specifically the curvature filters as a tool, will be useful in analyzing ECG signals corresponding to heart disorders which can significantly change the rhythm of the heart beat.

CONCLUSION

In the present work we propose a methodology for estimating the fiducial points of an ECG signal, partly based on an introduced tool for signal processing, the curvature filters. This task is expected to be continued in subsequent works. Concretely, one of our main research lines is continue to exploting the curvature filters and related tools potential for ECG analysis.

ETHICS APPROVAL AND CONSENT TO PARTICIPATE

Not applicable.

HUMAN AND ANIMAL RIGHTS

No Animals/Humans were used for studies that are base of this research.

CONSENT FOR PUBLICATION

Not applicable.

CONFLICT OF INTEREST

The authors declare no conflict of interest, financial or otherwise.

APPENDIX A

Proofs

In this section we provide proofs for Proposition 2.1 and Proposition 2.3.

Proof of Proposition 2.1: we recall that the values for the scaling factors in the definition of curvature filters (6) are provided in (7). The argument is a combination of ideas from Elementary Arithmetic, and goes as follows: for any p,

from equation (4) we obtain an expression for $f_{12m+p,k}$ by factorizing $\widetilde{f}_{12m+p,k} = \lambda_{12m+p} f_{12m+p,k}$ for k=1,...,12$m+p$,

and we make sure that $\{f_{12m+p,k}\}_{k=1}^{12m+p}$ are integers.

Next, we prove that they are mutually prime. If some integer is a common divisor of the filter entries, then has to divide any difference of them. Particularly we compute the difference of two consecutive central entries, around the index value $(n+1)/2$, because of they are the mutually closest ones. By using this fact we reduce the list of candidates so much. From this, it is straightforward to check there is no common divisors different from +1 or -1.

Details are shown up next for every case:

● **p=0:** we have $\lambda_{12m} = 2$ and for k=1,...,12m

$$f_{12m,k} = 2\left(36\,m^2 + 9\,m - 18\,mk + \frac{3k(k-1)}{2}\right) + 1 = 3\left(24\,m^2 + 6\,m - 12\,mk + k^2 - k\right) + 1. \qquad \textbf{(23)}$$

Since $f_{12m,6m+2}$-$f_{12m,6m+1}$ = 6, the common divisors divide 6. But 2 nor 3 divide no $f_{12m,k}$. Note that $k(k\text{-}1)$ is even for any integer k.

- **p+1:** we have λ_{12m+1} = 6 and for k=1,...,12m+1

$$f_{12m+1,k} = 3\left(8m^2 - 4mk + \frac{10m + k^2 - 2k + 1}{3}\right).$$

(24)

Since $f_{12m+1,6m+2}$-$f_{12m+1,6m+1}$ = 3, the common divisors divide 3. If 3 divides m, then it is easily seen that 3 does not divide $f_{12m+1,2}$, and if 3 does not divide m, one can easily check that 3 does not divide $f_{12m+1,1}$.

- **p=2:** we have λ_{12m+2} = 12 and for k=1,...,12m+2

$$f_{12m+2,k} = 12m^2 + 7m - 6mk + \frac{k(k-3)}{2} + 1.$$

(25)

Note that $k(k\text{-}3)$ is even for any integer k. Since $f_{12m+2,6m}$-$f_{12m+2,6m+1}$ = 1, we have finished.

- **p=3:** we have λ_{12m+3} = 2 and for k=1,...,12m+3

$$f_{12m+3,k} = 3\left(24m^2 + 18m - 12mk + k^2 - 4k\right) + 10.$$

(26)

Since $f_{12m+3,6m+1}$-$f_{12m+3,6m+2}$ = 3, the common divisors divide 3, but 3 divide no $f_{12m+3,k}$.

- **p=4:** we have λ_{12m+4} = 6 and for k=1,...,12m+4

$$f_{12m+4,k} = 24m^2 + 22m - 12mk + k^2 - 5k + 5.$$

(27)

Since $f_{12m+4,6m+1}$-$f_{12m+4,6m+2}$ = 1, we have finished.

- **p=5:** we have λ_{12m+5} = 6 and for k=1,...,12m+5

$$f_{12m+5,k} = 24m^2 + 26m - 12mk + k^2 - 6k + 7.$$

(28)

Since $f_{12m+5,6m+2}$-$f_{12m+5,6m+3}$ = 1, we have finished.

- **p=6:** we have λ_{12m+6} = 4 and for k=1,...,12m+6

$$f_{12m+6,k} = 3\left(12m^2 + 15m - 6mk + \frac{k(k-7)}{2}\right) + 14.$$

(29)

Since $f_{12m+6,6m+2}$-$f_{12m+6,6m+3}$ = 3, the common divisors divide 3, but 3 divide no $f_{12m+6,k}$. Note that $k(k\text{-}7)$ is even for any integer k.

- **p=7:** we have λ_{12m+7} = 6 and for k=1,...,12m+7

$$f_{12m+7,k} = 24m^2 + 34m - 12mk + k^2 - 8k + 12.$$

(30)

Since $f_{12m+7,6m+3}$-$f_{12m+7,6m+4}$ = 1, we have finished.

- **p=8:** we have λ_{12m+8} = 6 and for k=1,...,12m+8

$$f_{12m+8,k} = 2\left(12m^2 + 19m - 6mk\right) + k^2 - 9k + 15,$$

(31)

Since $f_{12m+8,6m+3}$-$f_{12m+8,6m+4}$ = 2, the common divisors divide 2, but $f_{12m+8,2}$ is odd.

- **p=9:** we have λ_{12m+9} = 2 and for k=1,...,12m+9

$$f_{12m+9,k} = 3\left(24m^2 + 42m - 12mk + k^2 - 10k\right) + 55. \tag{32}$$

Since $f_{12m+9,6m+4}$-$f_{12m+9,6m+5} = 3$, the common divisors divide 3, but 3 divide no $f_{12m+9,k}$.

● **p=10:** we have $\lambda_{12m+10} = 12$ and for $k=1,...,12m+10$

$$f_{12m+10,k} = 12m^2 + 23m - 6mk + \frac{k(k-11)}{2} + 11. \tag{33}$$

Note that $k(k\text{-}11)$ is even for any integer k. Since $f_{12m+10,6m+4}$-$f_{12m+10,6m+5} = 1$, we have finished.

● **p=11:** we have $\lambda_{12m+11} = 6$ and for $k=1,...,12m+11$

$$f_{12m+11,k} = 24m^2 + 50m - 12mk + k^2 - 12k + 26. \tag{34}$$

Since $f_{12m+11,6m+5}$-$f_{12m+11,6m+6} = 1$, we have finished.

Proof of Proposition 2.3: from (5) we have

$$\sum_{v=1}^{n} |\widetilde{f}_{n,v}|^2 = \sum_{v=1}^{n} \left| 6\left(v - \frac{n+1}{2}\right)^2 - \frac{n^2-1}{2} \right|^2 = \tag{35}$$

$$= 36 \sum_{v=1}^{n} \left(v - \frac{n+1}{2}\right)^4 - 6(n^2-1) \sum_{v=1}^{n} \left(v - \frac{n+1}{2}\right)^2 + \frac{1}{4}n(n^2-1)^2. \tag{36}$$

Now we compute these two sums separately. On the one hand,

$$\sum_{v=1}^{n} \left(v - \frac{n+1}{2}\right)^2 = \left(\frac{1}{6}\sum_{v=1}^{n}\widetilde{f}_{n,v}\right) + \frac{n(n^2-1)}{12} = \frac{n(n^2-1)}{12}. \tag{37}$$

In order to compute the other sum, we split in two cases. We will make use of the well known Faulhaber formulas: for any positive integer N, one has

$$\sum_{j=1}^{N} j = \frac{N^2+N}{2}, \qquad \sum_{j=1}^{N} j^2 = \frac{2N^3+3N^2+N}{6}, \tag{38}$$

$$\sum_{j=1}^{N} j^3 = \frac{N^4+2N^3+N^2}{4}, \qquad \text{and} \qquad \sum_{j=1}^{N} j^4 = \frac{6N^5+15N^4+10N^3-N}{30}. \tag{39}$$

If n is odd, then there exists a positive integer m such that $n=2m\text{-}1$. Then

$$\sum_{v=1}^{n} \left(v - \frac{n+1}{2}\right)^4 = \sum_{v=1}^{2m-1}(v-m)^4 = 2\sum_{v=1}^{m-1} v^4 = \tag{40}$$

$$= \frac{1}{80}n^5 - \frac{1}{24}n^3 + \frac{7}{240}n = \frac{3n^5 - 10n^3 + 7n}{240}. \tag{41}$$

On the other hand, if n is even, then there exists a positive integer m such that $n=2m$. Then

$$\sum_{v=1}^{n} \left(v - \frac{n+1}{2} \right)^4 = \sum_{v=1}^{2m} \left(v - m - \frac{1}{2} \right)^4 = 2 \sum_{v=0}^{m-1} \left(v + \frac{1}{2} \right)^4 = \tag{42}$$

$$= 2 \sum_{v=0}^{m-1} \left(v^4 + 2 v^3 + \frac{3}{2} v^2 + \frac{1}{2} v + \frac{1}{16} \right) = \tag{43}$$

$$= \frac{1}{80} n^5 - \frac{1}{24} n^3 + \frac{7}{240} n = \frac{3 n^5 - 10 n^3 + 7 n}{240} . \tag{44}$$

Note that in both cases we obtain the same expression.

Finally, we have

$$\|\widetilde{f_n}\|^2 = 36 \frac{3 n^5 - 10 n^3 + 7 n}{240} - 6 (n^2 - 1) \frac{n(n^2 - 1)}{12} + \frac{1}{4} n (n^2 - 1)^2 = \tag{45}$$

$$= \frac{n^5 - 5 n^3 + 4 n}{5} = \frac{(n-2)(n-1) n (n+1)(n+2)}{5} . \tag{46}$$

REFERENCES

[1]   Sörnmo L, Laguna P. Bioelectrical signal processing in cardiac and neurological applications. Amsterdam, Boston: Elsevier Academic Press 2005.

[2]   Clifford GD, Azuaje F, McSharry PE, Eds. Advanced methods and tools for ECG analysis. Artech House Publishing October 2006.

[3]   Karpagachelvi S, Arthanari M, Sivakumar M. ECG feature extraction techniques: A survey approach. Int J Comp Sci Inf Security 2010; 8(1)

[4]   Beraza I, Romero I. Comparative study of algorithms for ECG segmentation. Biomed Signal Process Control 2017; 34: 166-73.
        [http://dx.doi.org/10.1016/j.bspc.2017.01.013]

[5]   Will C, Shi K, Weigel R, Koelpin A. Advanced template matching algorithm for instantaneous heartbeat detection using continuous wave radar systems. In: Microwave Bio Conference (IMBIOC), 2017 First MTT-S Int. 2017; pp. 1-4. IEEE
        [http://dx.doi.org/10.1109/IMBIOC.2017.7965797]

[6]   Will C, Shi K, Schellenberger S, *et al.* Local pulse wave detection using continuous wave radar systems. IEEE J Electromagn, RF Microwaves Med Biol 2017; 1(2): 81-9.
        [http://dx.doi.org/10.1109/JERM.2017.2766567]

[7]   Shi K, Will C, Steigleder T, *et al.* A contactless system for continuous vital sign monitoring in palliative and intensive care. In: Systems Conference (SysCon). Annual IEEE Int. 2018; pp. 1-8.
        [http://dx.doi.org/10.1109/SYSCON.2018.8369507]

[8]   Shi K, Will C, Weigel R, Koelpin A. Contactless person identification using cardiac radar signals. In: IEEE International Instrumentation and Measurement Technology Conference (I2MTC). 2018. IEEE
        [http://dx.doi.org/10.1109/I2MTC.2018.8409645]

[9]   Wang Y, Agrafioti F, Hatzinakos D, Plataniotis KN. Analysis of human electrocardiogram for biometric recognition. EURASIP J Adv Signal Process 2007; 2008(1): 148658.
        [http://dx.doi.org/10.1155/2008/148658]

[10]   Garcia-Baleon HA, Alarcon-Aquino V, Starostenko O. A wavelet-based 128-bit key generator using electrocardiogram signals 52nd IEEE International Midwest Symposium Circuits and Systems. 644-7.

[11]   Bui FM, Agrafioti F, Hatzinakos D. Electrocardiogram (ECG) biometric for robust identification and secure communication. Biom Theory Methods Appl 2009; 9: 383.

[12]   Shi J, Lam KY. Vitacode: Electrocardiogram representation for biometric cryptography in body area networks. In: First International Conference on Ubiquitous and Future Networks. Hong Kong 2009; pp. 112-5.
        [http://dx.doi.org/10.1109/ICUFN.2009.5174295]

[13]   Yao L, Liu B, Yao K, Wu G, Wang J. An ECG-Based signal key establishment protocol in body area networks. 7th International Conference on Ubiquitous Intelligence & Computing and 7th International Conference on Autonomic & Trusted Computing, Xian, Shaanxi 2010; 233-8.
        [http://dx.doi.org/10.1109/UIC-ATC.2010.7]

[14]   Belgacem N, Nait-Ali A, Fournier R, Bereksi-Reguig F. ECG based human authentication using wavelets and random forests. Int J Cryptogr Inf Secur 2012; 2(3): 1-11.

[15]   Damaševičius R, Maskeliūnas R, Kazanavičius E, Woźniak M. Combining Cryptography with EEG Biometrics. Comput Intell Neurosci 2018; 1867548.
[http://dx.doi.org/10.1155/2018/1867548] [PMID: 29951089]

[16]   Ring C, Brener J. Heartbeat counting is unrelated to heartbeat detection: A comparison of methods to quantify interoception. Psychophysiology 2018; 55(9): e13084.
[http://dx.doi.org/10.1111/psyp.13084] [PMID: 29633292]

[17]   Pande VN, Verma HK, Mukhopadhyay P. Software detection of ECG baseline and *QRS*-complex for coronary intensive care. J Microcomp Applicat 1985; 8(3): 203-14.
[http://dx.doi.org/10.1016/0745-7138(85)90001-6]

[18]   Tompkins WJ, Ed. Biomedical digital signal processing: C-language examples and laboratory experiments for the IBM PC. Englewood Cliffs, NJ: Prentice-Hall 1993.

[19]   Köhler B-U, Hennig C, Orglmeister R. The principles of software *QRS* detection. IEEE Eng Med Biol Mag 2002; 21(1): 42-57.
[http://dx.doi.org/10.1109/51.993193] [PMID: 11935987]

[20]   Martínez JP, Almeida R, Olmos S, Rocha AP, Laguna P. A wavelet-based ECG delineator: Evaluation on standard databases. IEEE Trans Biomed Eng 2004; 51(4): 570-81.
[http://dx.doi.org/10.1109/TBME.2003.821031] [PMID: 15072211]

[21]   Addison PS. Wavelet transforms and the ECG: A review. Physiol Meas 2005; 26(5): R155-99.
[http://dx.doi.org/10.1088/0967-3334/26/5/R01] [PMID: 16088052]

[22]   Zhang Q, Manriquez AI, Médigue C, Papelier Y, Sorine M. An algorithm for robust and efficient location of T-wave ends in electrocardiograms. IEEE Trans Biomed Eng 2006; 53(12 Pt 1): 2544-52.
[http://dx.doi.org/10.1109/TBME.2006.884644] [PMID: 17153212]

[23]   Altuve M, Casanova O, Wong S, Passariello G, Hernández A, Carrault G. Evaluación de dos métodos para la segmentación del ancho de la onda T en el ECG. IFMBE Proc 2007; 18: 1254-8.
[http://dx.doi.org/10.1007/978-3-540-74471-9_291]

[24]   Parák J, Havlík J. ECG signal processing and heart rate frequency detection methods. Proceedings of the 19th Annual Conference Technical Computing Prague 2011; 91-6.

[25]   Laguna P, Thakor NV, Caminal P, *et al.* New algorithm for*QT*interval analysis in 24-hour Holter ECG: Performance and applications. Med Biol Eng Comput 1990; 28(1): 67-73.
[http://dx.doi.org/10.1007/BF02441680] [PMID: 2325452]

[26]   Murthy ISN, Niranjan UC. Component wave delineation of ECG by filtering in the Fourier domain. Med Biol Eng Comput 1992; 30(2): 169-76.
[http://dx.doi.org/10.1007/BF02446127] [PMID: 1453782]

[27]   Laguna P, Jané R, Caminal P. Automatic detection of wave boundaries in multilead ECG signals: Validation with the CSE database. Comput Biomed Res 1994; 27(1): 45-60.
[http://dx.doi.org/10.1006/cbmr.1994.1006] [PMID: 8004942]

[28]   Li C, Zheng C, Tai C. Detection of ECG characteristic points using wavelet transforms. IEEE Trans Biomed Eng 1995; 42(1): 21-8.
[http://dx.doi.org/10.1109/10.362922] [PMID: 7851927]

[29]   De Chazal P, Celler BG. Automatic measurement of the *QRS* onset and offset in individual ECG leads Proceedings of the 18th Annual Int Conf IEEE. 4: 1399-400.

[30]   Jane R, Blasi A, García J, Laguna P. Evaluation of an automatic threshold based detector of waveform limits in Holter ECG with the *QT* database. Comput Cardiol 1997; 295-8.

[31]   Sahambi JS, Tandon SN, Bhatt RKP. Using wavelet transforms for ECG characterization. An on-line digital signal processing system. IEEE Eng Med Biol Mag 1997; 16(1): 77-83.
[http://dx.doi.org/10.1109/51.566158] [PMID: 9058586]

[32]   Vullings HJLM, Verhaegen MHG, Verbruggen HB. Automated ECG segmentation with dynamic time warping Proceedings of the 20th Annu Int Conf IEEE 1998; 163-6.
[http://dx.doi.org/10.1109/IEMBS.1998.745863]

[33]   Afonso VX, Tompkins WJ, Nguyen TQ, Luo S. ECG beat detection using filter banks. IEEE Trans Biomed Eng 1999; 46(2): 192-202.
[http://dx.doi.org/10.1109/10.740882] [PMID: 9932341]

[34]   Vila JA, Gang Y, Rodriguez Presedo JM, Fernández-Delgado M, Barro S, Malik M. A new approach for TU complex characterization. IEEE Trans Biomed Eng 2000; 47(6): 764-72.
[http://dx.doi.org/10.1109/10.844227] [PMID: 10833851]

[35]   Martinez JP, Olmos S, Laguna P. Evaluation of a wavelet-based ECG waveform detector on the *QT* database. Comput Cardiol 2000; 81-4.
[IEEE.].

[36]   Schreier G, Hayn D, Lobodzinski S. Development of a new *QT* algorithm with heterogenous ECG databases. J Electrocardiol 2003; 36(Suppl.): 145-50.
[http://dx.doi.org/10.1016/j.jelectrocard.2003.09.039] [PMID: 14716616]

[37]   Last T, Nugent CD, Owens FJ. Multi-component based cross correlation beat detection in electrocardiogram analysis. Biomed Eng Online 2004; 3(1): 26.
[http://dx.doi.org/10.1186/1475-925X-3-26] [PMID: 15272931]

[38]   Sun Y, Chan KL, Krishnan SM. Characteristic wave detection in ECG signal using morphological transform. BMC Cardiovasc Disord 2005; 5(1): 28.
[http://dx.doi.org/10.1186/1471-2261-5-28] [PMID: 16171531]

[39]   Mahmoodabadi SZ, Ahmadian A, Abolhasani MD. ECG feature extraction using Daubechies wavelets. Proceedings of the fifth IASTED International conference on Visualization, Imaging and Image Processing. 343-8.

[40]   Dumont J, Hernandez AI, Carrault G. Parameter optimization of a wavelet-based electrocardiogram delineator with an evolutionary algorithm. Comput Cardiol 2005; 707-10. [IEEE.].

[41]   Thomas J, Rose C, Charpillet F. A multi-HMM approach to ECG segmentation. 18th IEEE International Conference on Tools with Artificial Intelligence 2006; 609-16.

[42]   Zifan A, Saberi S, Moradi MH, Towhidkhah F. Automated ECG segmentation using piecewise derivative dynamic time warping. Int J Biological Medical Sci 2006; 1(3)

[43]   Andreão RV, Dorizzi B, Boudy J. ECG signal analysis through hidden Markov models. IEEE Trans Biomed Eng 2006; 53(8): 1541-9.
[http://dx.doi.org/10.1109/TBME.2006.877103] [PMID: 16916088]

[44]   Manriquez AI, Zhang Q. n algorithm for QRS onset and offset detection in single lead electrocardiogram records In: Engineering in Medicine and Biology Society. EMBS 2007. 29th Annual International Conference of the IEEE 2007; 541-4.
[http://dx.doi.org/10.1109/IEMBS.2007.4352347]

[45]   Madeiro JP, Cortez PC, Oliveira FI, Siqueira RS. A new approach to *QRS* segmentation based on wavelet bases and adaptive threshold technique. Med Eng Phys 2007; 29(1): 26-37.
[http://dx.doi.org/10.1016/j.medengphy.2006.01.008] [PMID: 16500133]

[46]   Thomas J, Rose C, Charpillet F. A support system for ECG segmentation based on Hidden Markov Models In: Engineering in Medicine and Biology Society. EMBS 2007. Ann Int Conf IEEE 2007; 3228-1.
[http://dx.doi.org/10.1109/IEMBS.2007.4353017]

[47]   Illanes-Manriquez A, Zhang Q. An algorithm for robust detection of *QRS* onset and offset in ECG signals. Comput Cardiol 2008; 857-60. [IEEE.].

[48]   Krimi S, Ouni K, Ellouze N. An approach combining wavelet transform and hidden Markov models for ECG segmentation. 3rd International Conference on Information and Communication Technologies: From Theory to Applications 2008; 1-6.

[49]   Ghaffari A, Golbayani H, Ghasemi M. A new mathematical based *QRS* detector using continuous wavelet transform. Comput Electr Eng 2008; 34(2): 81-91.
[http://dx.doi.org/10.1016/j.compeleceng.2007.10.005]

[50]   Frénay B, de Lannoy G, Verleysen M. Emission modelling for supervised ECG segmentation using finite differences 4th European Conference of the International Federation for Medical and Biological Engineering 1212-6.2009;
[http://dx.doi.org/10.1007/978-3-540-89208-3_290]

[51]   Almeida R, Martínez JP, Rocha AP, Laguna P. Multilead ECG delineation using spatially projected leads from wavelet transform loops. IEEE Trans Biomed Eng 2009; 56(8): 1996-2005.
[http://dx.doi.org/10.1109/TBME.2009.2021658] [PMID: 19447698]

[52]   de Lannoy G, Frénay B, Verleysen M, Delbeke J. Supervised ECG delineation using the wavelet transform and hidden Markov models 4th European Conference of the International Federation for Medical and Biological Engineering. 22-5.
[http://dx.doi.org/10.1007/978-3-540-89208-3_7]

[53]   Illanes-Manriquez A. An automatic multi-lead electrocardiogram segmentation algorithm based on abrupt change detection Engineering in Medicine and Biology Society (EMBC). 2334-7.
[http://dx.doi.org/10.1109/IEMBS.2010.5627473]

[54]   Martínez A, Alcaraz R, Rieta JJ. Application of the phasor transform for automatic delineation of single-lead ECG fiducial points. Physiol Meas 2010; 31(11): 1467-85.
[http://dx.doi.org/10.1088/0967-3334/31/11/005] [PMID: 20871135]

[55]   Vítek M, Hrubeŝ J, Kozumplík J. A wavelet-based ECG delineation with improved P wave offset detection accuracy. Anal Biomed Signals Images 2010; 20: 1-6.

[56]   Shi W, Kheidorov I. Hybrid hidden Markov models for ECG segmentation. 6th International Conference on Natural Computation 2010; 3323-8.

[57]   Dumont Ast J, Hernández AI, Carrault G. Improving ECG beats delineation with an evolutionary optimization process. IEEE Trans Biomed Eng 2010; 57(3): 607-15.

[http://dx.doi.org/10.1109/TBME.2008.2002157] [PMID: 19171513]

[58] Ghaffari A, Homaeinezhad MR, Khazraee M, Daevaeiha MM. Segmentation of holter ECG waves *via* analysis of a discrete wavelet-derived multiple skewness-kurtosis based metric. Ann Biomed Eng 2010; 38(4): 1497-510.
[http://dx.doi.org/10.1007/s10439-010-9919-3] [PMID: 20087769]

[59] Llamedo M, Martínez JP. Heartbeat classification using feature selection driven by database generalization criteria. IEEE Trans Biomed Eng 2011; 58(3): 616-25.
[http://dx.doi.org/10.1109/TBME.2010.2068048] [PMID: 20729162]

[60] Gupta R, Mitra M, Mondal K, Bhowmick S. A derivative-based approach for QT-segment feature extraction in digitized ECG record. Second International Conference on Emerging Applications of Information Technology (EAIT) 2011; 63-.
[http://dx.doi.org/10.1109/EAIT.2011.61]

[61] Homaeinezhad MR, Ghaffari A, Najjaran TH, Tahmasebi M, Daevaeiha MM. A unified framework for delineation of ambulatory holter ECG events via analysis of a multiple-order derivative wavelet-based measure. Iran J Electrical Electronic Eng 2011; 7(1): 1-18.

[62] Di Marco LY, Chiari L. A wavelet-based ECG delineation algorithm for 32-bit integer online processing. Biomed Eng Online 2011; 10(1): 23.
[http://dx.doi.org/10.1186/1475-925X-10-23] [PMID: 21457580]

[63] Rincón F, Recas J, Khaled N, Atienza D. Development and evaluation of multilead wavelet-based ECG delineation algorithms for embedded wireless sensor nodes. IEEE Trans Inf Technol Biomed 2011; 15(6): 854-63.
[http://dx.doi.org/10.1109/TITB.2011.2163943] [PMID: 21827976]

[64] Mukhopadhyay SK, Mitra M, Mitra S. Time plane ECG feature extraction using hilbert transform, variable threshold and slope reversal approach In: Communication and Industrial Application (ICCIA). IEEE. 2011; pp. 1-4.
[http://dx.doi.org/10.1109/ICCIndA.2011.6146675]

[65] Madeiro JP, Cortez PC, Marques JA, Seisdedos CR, Sobrinho CR. An innovative approach of *QRS* segmentation based on first-derivative, Hilbert and Wavelet Transforms. Med Eng Phys 2012; 34(9): 1236-46.
[http://dx.doi.org/10.1016/j.medengphy.2011.12.011] [PMID: 22226589]

[66] Manikandan MS, Soman KP. A novel method for detecting R-peaks in electrocardiogram (ECG) signal. Biomed Signal Process Control 2012; 7(2): 118-28.
[http://dx.doi.org/10.1016/j.bspc.2011.03.004]

[67] Beraza Azurmendi I. Comparative study of algorithms for segmentation of the electrocardiogram signal. 2012.

[68] Li T, Zhou M. ECG classification using wavelet packet entropy and random forests. Entropy (Basel) 2016; 18(8): 285.
[http://dx.doi.org/10.3390/e18080285]

[69] Chan HL, Wang FT, Lee YS, Wang CL. Heartbeat detection using oscillatory envelope pattern in noisy electrocardiogram. Computing 2017; 44: 1.

[70] Guyton AC, Hall JE. Treaty of medical physiology. 2nd ed. NY, USA: Elsevier 2011.

[71] My EKG. The web of the electrocardiogram http://www.my-ekg.com/

[72] Sequence of changes in myocardial infarction https:// www.oru.se/ english/ schools/ health-sciences/

[73] Goldberger A L, Amaral L A N, Glass L, *et al.* PhysioBank, Physio Tool kit, and PhysioNet: Components of a new research resource for complex physiologic signals. Circulation 2000 (June 13); 101(23): e215-20. Circulation Electronic Pages; http://circ.ahajournals.org/content/.
[http://dx.doi.org/10.1161/01.CIR.101.23.e215]

[74] MATLAB. The language of technical computing General documentation, DSP System Toolbox Releases R2013a & R2011b Available from: https://www.mathworks.com/help/matlab/.

[75] Cardiosim II. ECG arrhytmia simulator Operating Instruction.

[76] Sklar B. Digital communications: Fundamentals and applications 2nd Ed. Prentice Hall: University of California 2001.

[77] Scott P. Uncertainty in measurements: Noise and how to deal with it unpublished. Available at: Peter Scott's home page University of California Santa Cruz http://physics.ucsc.edu/~drip/133/ch2.pdf. 2017

[78] John W Eaton, David Bateman, Søren Hauberg, Rik RikWehbring. GNU Octave version 400 manual: A high-level interactive language for numerical computations. Available from: http://www.gnu.org/software/octave/doc/interpreter/